Influence of PWM on Trajectory Accuracy in Mobile Robot MOTION

Ryszard Beniak, Tomasz Pyka

Abstract:

The paper compares simulation results for direct and PWM control of DC motors in a tri-wheel mobile robot with a castor sliding wheel. Our aim was to determine to what extent PWM control changes the trajectory accuracy. For this purpose, we compare kinematic and dynamic control. To make the model more realistic, we considered the impact of viscous and rolling friction of driving wheels on the motion along the trajectory. We conclude that dynamic control is of higher quality as compared to kinematic control, and that there is a significant impact of PWM control on the trajectory accuracy.

Keywords: *mobile robot control, kinematic and dynamic control, castor sliding wheel, pulse width modulation.*

1. Introduction

The issue of trajectory accuracy has not been yet resolved for mobile robots with to a satisfactory extent. The regulator is incapable to determine the trajectory accurately enough given surface irregularities impacting the behaviour of wheels. For this reason, the theoretical and empirical trajectories might deviate from each other significantly. The impact of slips on the trajectory has been considered in [1, 2, 3, 4] for tri-wheel robots, in [5] for four-wheel robots and in [6] for unicycles. Not considering wheel slips might lead to significant trajectory errors [7, 8, 9, 10]. Yet, for simulation of trajectory of tri-wheel robots, the castor free wheel is assumed to be passive [11] and not to have any impact on the trajectory.

In this paper, we consider a tri-wheel robot with a castor sliding wheel [12]. The innovation is that the castor wheel does exert an impact on the entire mobile robot. Viscous and rolling frictions do influence the motion of the castor wheel. Friction coefficients are assumed to have normal distribution *N(0.001, 0.00058)*. The simulation was carried out for an example trajectory as in [12] rotation around a fixed axis (Fig. 5), i.e. around a characteristic point A (Fig.1). For simulation purposes, we assumed the parameters of a Dunkermotoren GR63x25 motor with a PLG52 1:36 transmission.

Next, we compared the kinematic and dynamic control for both direct (without any modulation) and PWM control types [13]. [6] contains a comparison between kinematic and dynamic control, though without any restriction imposed on torques and forces. Kinematic [14] and dynamic control are still applied in robotics [10], though they are increasingly often combined with adaptive [11] and robust control.

2. Mobile robot model

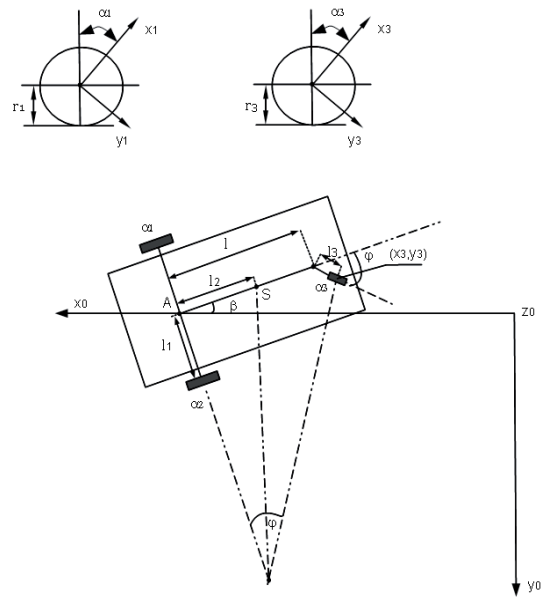Simulations were carried out for the model presented in Fig. 1:

Fig. 1. Tree-wheeled robot with a castor rear wheel

where S – center of frame mass, A – characteristic point, l – distance between the characteristic point and arm of the castor wheel, l_1 – distance from characteristic point to driving wheel, l_2 – distance between center of frame mass and the characteristic point, l_3 – length of the free wheel arm, β – rotary angle of the frame, φ – angle of the castor wheel along the axis y_3, α_1, α_2, α_3 – rotary angles of individual wheels along axis z_1, z_2 and z_3, respectively.

Mobile robot dynamic equation is described as follows:

$$\mathbf{M}(q)\ddot{\mathbf{q}} + \mathbf{C}(q,\dot{q})\dot{\mathbf{q}} = \mathbf{B}(q)\tau + \mathbf{J}^T(q)\lambda, \qquad (1)$$

where:

$$\ddot{\mathbf{q}}^T = \begin{bmatrix} \ddot{\beta} & \ddot{\psi} & \ddot{\varphi} & \ddot{\alpha}_3 \end{bmatrix},$$

$$\dot{\mathbf{q}}^T = \begin{bmatrix} \dot{\beta} & \dot{\psi} & \dot{\varphi} & \dot{\alpha}_3 \end{bmatrix},$$

$$\mathbf{M} = \begin{bmatrix} a_{11} & a_{12} & a_{13} & 0 \\ a_{21} & a_{22} & a_{23} & 0 \\ a_{31} & a_{32} & a_{33} & 0 \\ 0 & 0 & 0 & 0 \end{bmatrix}, \quad \mathbf{C} = \begin{bmatrix} c_{11} & c_{12} & c_{13} & 0 \\ c_{21} & c_{22} & c_{23} & 0 \\ c_{31} & c_{32} & c_{33} & 0 \\ 0 & 0 & 0 & c_{44} \end{bmatrix},$$

The elements of matrix **M** are described as:

$$a_{11} = m_3(l^2 + l_3^2 + 2l_3l\cos(\varphi)) + I_{y3} + 2h_1^2(m_1r_1^2 + I_{z1}) +$$

$$2I_{y1} + m_5l_2^2 + I_{z5}, \quad a_{12} = a_{21} = -m_3r_1l_3\sin(\varphi),$$

$$a_{23} = a_{32} = m_3r_1l_3\sin(\varphi),$$

$$a_{33} = m_3l_3^2 + I_{y3}, \quad a_{22} = m_3r_1^2 + 2m_1r_1^2 + 2I_{z1} + m_5r_1^2,$$

$$a_{13} = a_{31} = -m_3(l_3^2 + l_3l\cos(\varphi)) - I_{y3}.$$

The elements of C matrix are calculated as follows:

$$c_{11} = m_3(-3\dot{\varphi}l_3l\sin(\varphi) + \dot{\beta}l_3l\sin(\varphi)) + (N_1f_1 + N_2f_2)h_1^2,$$

$$c_{12} = m_3(-r_1l_3\cos(\varphi)(\dot{\varphi} - \dot{\beta}) - \dot{\varphi}r_1l_3\cos(\varphi)) + (N_1f_1 - N_2f_2)h_1,$$

$$c_{13} = m_3\dot{\varphi}l_3l\sin(\varphi) + D_\varphi, \quad c_{23} = m_3r_1l_3\cos(\varphi)(\dot{\varphi} - \dot{\beta}) + D_\varphi,$$

$$c_{21} = m_3(\dot{\beta}l_3l\sin(\varphi) - \dot{\varphi}l_3l\sin(\varphi)) + (N_1f_1 - N_2f_2)h_1,$$

$$c_{22} = -m_3r_1l_3\cos(\varphi)(\dot{\varphi} - \dot{\beta}) + (N_1f_1 + N_2f_2),$$

$$c_{31} = m_3\dot{\beta}l_3l\sin(\varphi), \quad c_{32} = m_3\dot{\beta}r_1l_3\cos(\varphi).$$

$$c_{33} = D_\varphi, \quad c_{44} = D_3r_3^2\cos\varphi + D_{\alpha3},$$

$$\mathbf{B}(q)\tau + \mathbf{J}^T(q)\lambda = \begin{cases} (M_1 - M_2)h_1 - N_3f_3l_3\sin(\varphi_c - \varphi)\upsilon \\ M_1 + M_2 - N_3f_3l_3\sin(\varphi_c - \varphi)\upsilon \\ -N_3f_3l_3\sin(\varphi_c - \varphi)\upsilon \\ \upsilon D_\varphi r_3\cos\varphi \end{cases}$$

where φ_c is the natural (non-sliding) angle of the castor wheel with sliding being exempted, R is the current radius of the trajectory and υ is the desired velocity of the castor sliding wheel. N_1, N_2, N_3 are the pressure wheels of the ground, respectively. M_1, M_2 are DC torques, f_1, f_2, f_3 are wheels coefficients friction of the ground, respectively and $D_\varphi, D_3, D_{\alpha3}$ are damping factors. Variables υ, R and φ_c are calculated from the formulas below:
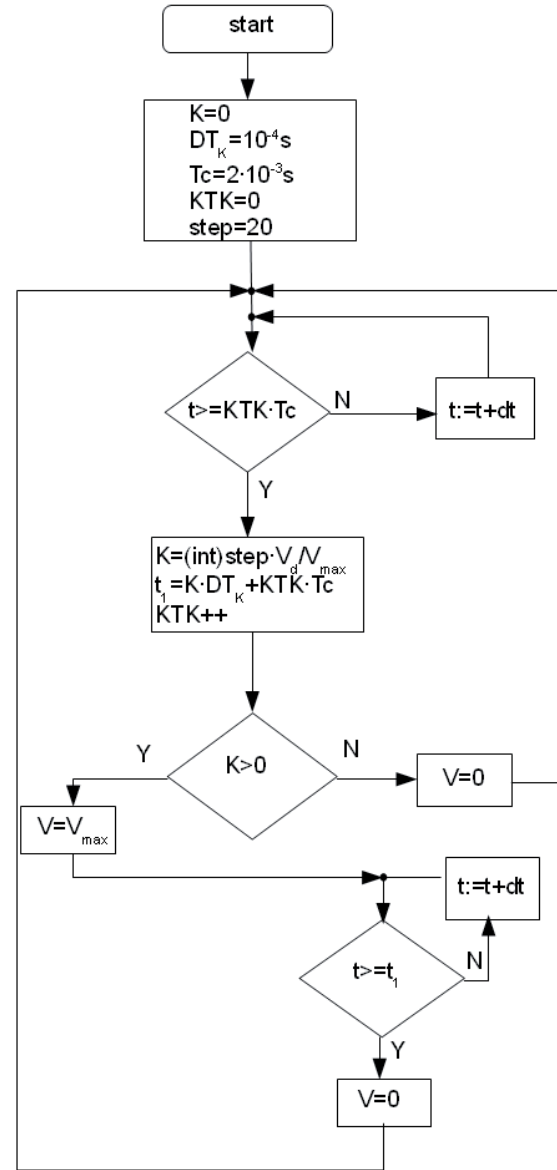

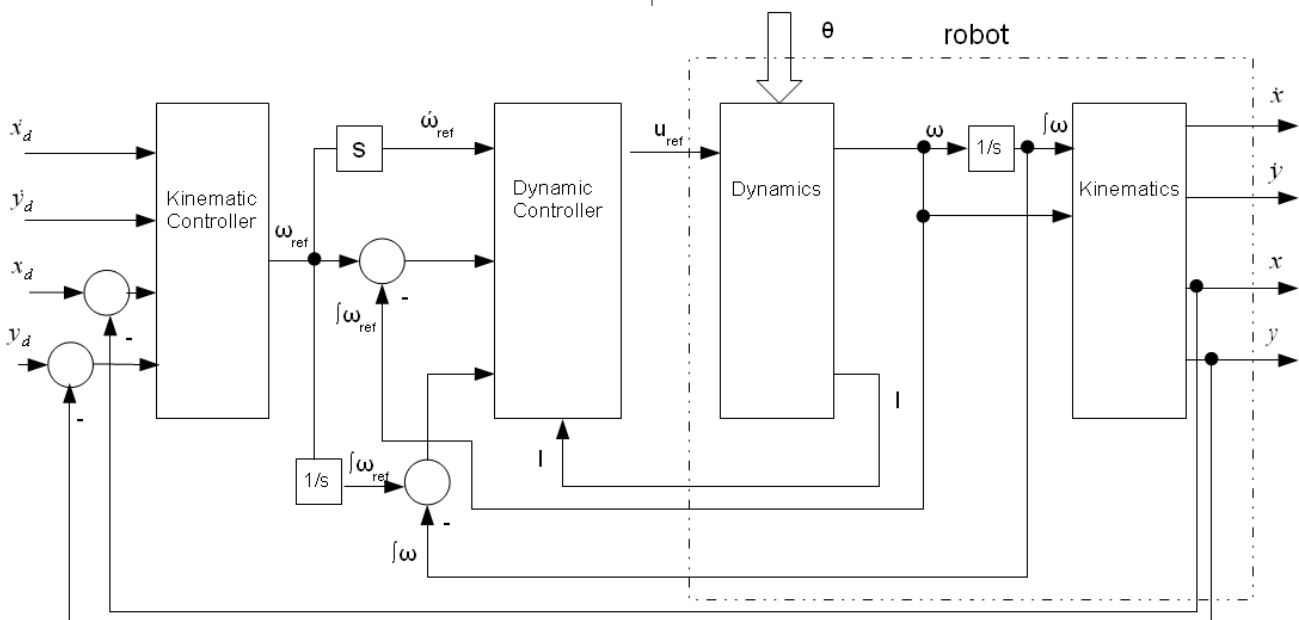Fig. 2. Algorithm of DC controller
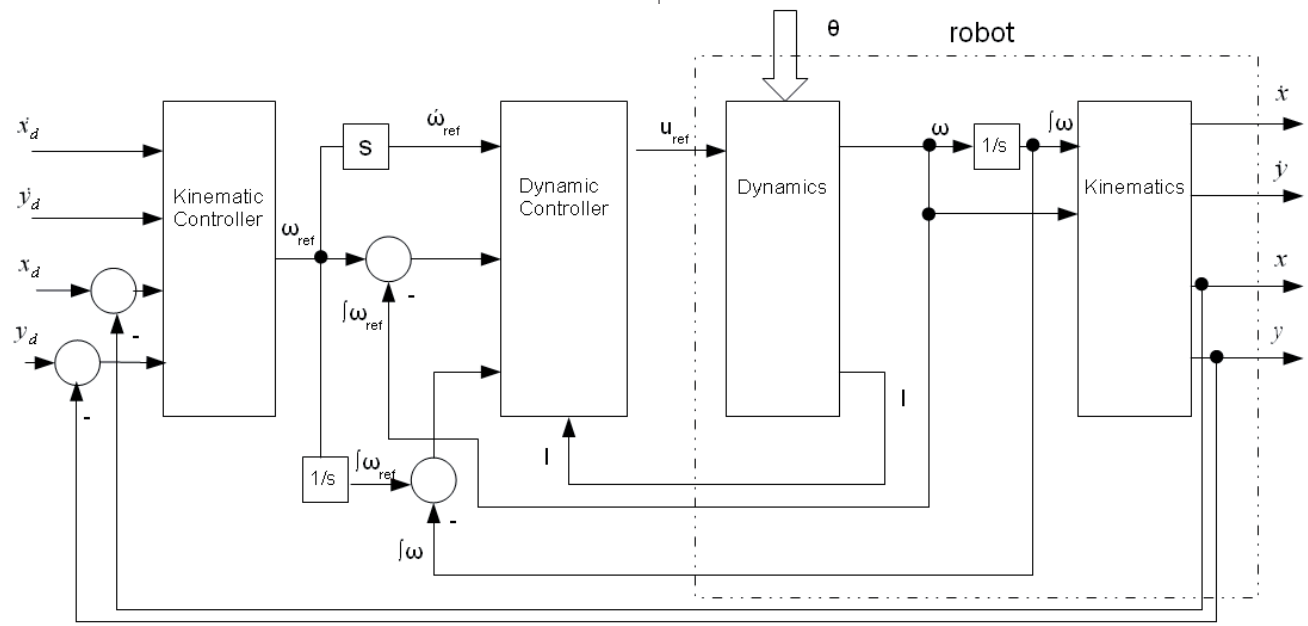

Fig. 3. Dynamic controller of the robot

Fig. 4. Kinematic controller of the robot

$$\varphi_c = a\cos\left(\frac{-l_3 l + \sqrt{(l^2 R^2 + R^4 - R^2 l_3^2)}}{l^2 + R^2}\right),$$

$$R = \frac{(\dot{x}^2 + \dot{y}^2)^{3/2}}{\begin{vmatrix} \dot{x} & \dot{y} \\ \ddot{x} & \ddot{y} \end{vmatrix}},$$

$$v = \sqrt{\left(r_1^2 \dot{\psi}^2 + l^2 \dot{\beta}^2 + l_3^2 (\dot{\varphi} - \dot{\beta})^2 + 2l_3(\dot{\varphi} - \dot{\beta})(r_1\dot{\psi}\sin(\varphi) - l\dot{\beta}\cos(\varphi))\right)}.$$

To make the model more realistic, we also modeled two transistor bridges H, each consisting of four transistors and four diodes. The algorithm which sets the instantaneous value of PWM voltages was presented in Fig. 2., where K is the duty cycle, DT_K – 1/20 of PWM impulse duration , V_{d1}, V_{d2} – voltages set by the regulator based on the set-torque M_{d1} and M_{d2}, V_{max} – maximum voltage (V_{max} = 24V), V_{min} – minimum voltage (V_{min} = 0V). Moreover, we assumed that the duration of a single PWM impulse Tc is 2 ms and that we do not take commutation process into account, dt – timestep.

The voltages V_{d1} and V_{d2} are calculated as follows:

$$V_{d1} = R_{a1} M_{d1} / (k\Psi) + k\Psi\dot{\alpha}_1,$$
$$V_{d2} = R_{a2} M_{d2} / (k\Psi) + k\Psi\dot{\alpha}_2, \qquad (2)$$

where Ψ_1, Ψ_2 – exciting flux, k – gear, $\dot{\alpha}_1 = \dot{\psi} + \dot{\beta}h_1$ and $\dot{\alpha}_2 = \dot{\psi} - \dot{\beta}h_1$ – driving wheels velocities.

To the robot dynamics equations (1) described above we added equations describing DC motors [15]:

$$\ddot{Q}_1 = (V_1 - R_{a1}\dot{Q}_1 - e_{a1}) / L_a,$$
$$\ddot{Q}_2 = (V_2 - R_{a2}\dot{Q}_2 - e_{a2}) / L_a, \qquad (3)$$

where $\dot{Q}_1, \dot{Q}_2$ – currents, e_{a1}, e_{a2} – inducted voltages, L_a – armature inductance.

Inducted voltages are equal to:

$$e_1 = k\Psi_1\dot{\alpha}_1, \; e_2 = k\Psi_2\dot{\alpha}_2, \qquad (4)$$

The motor armature resistances and voltages are calculated as:

$$R_{a1} = R_a + R_{c1},$$
$$R_{a2} = R_a + R_{c2}, \qquad (5)$$

$$R_{c1} = \sum_{i=1}^{4} \delta_{Ti} R_{Ti} + \sum_{j=1}^{4} \delta_{Dj} R_{Dj}, \qquad (6)$$

$$R_{c2} = \sum_{i=1}^{4} \delta_{Ti} R_{Ti} + \sum_{j=1}^{4} \delta_{Dj} R_{Dj}. \qquad (7)$$

$$\Delta V_{c1} = \sum_{i=1}^{4} \delta_{Ti} V_{C(TO)} + p\sum_{j=1}^{4} \delta_{Dj} V_{F(TO)}, \qquad (8)$$

$$\Delta V_{c2} = \sum_{i=1}^{4} \delta_{Ti} V_{C(TO)} + p\sum_{j=1}^{4} \delta_{Dj} V_{F(TO)}, \qquad (9)$$

$$V_1 = V - \Delta V_{c1}, \; V_2 = V - \Delta V_{c2}, \qquad (10)$$

where R_{a1} – resultant resistance of motor 1, R_{a2} – resultant resistance of motor 2, R_a – armature resistance, R_{c1}, R_{c2} – 1st and 2nd H-structure inverter resistance, V_{c1}, V_{c2} – first and second H-structure inverter voltage reduction, V – voltage value at source, $V_{C(TO)}$ – forward voltage of transistor, $V_{F(TO)}$ – forward voltage of diode, δ – Kronecker delta, i, j – indexes, T – transistor, D – diode, $V \in \{0, 24\}$ where V = 24V while two transistors or two diodes conducting (factor $p = -1$) and V = 0V in other cases (factor $p = 1$). If any $\delta_T = 1$ or $\delta_D = 1$, that means transistor or diode conducted.

The torques used in (1) are calculated as:

$$M_1 = k\Psi\dot{Q}_1, \quad M_2 = k\Psi\dot{Q}_2. \tag{11}$$

For dynamic and kinematic control (Fig. 4 and Fig. 5) $\dot{x}_d$, $\dot{y}_d$ are desired velocities of the characteristic point A as in Fig. 1., $\dot{x}$, $\dot{y}$ are output velocities of the characteristic point A, x_d, y_d are desired positions of the characteristic point A, ω is the vector of general coordinates,
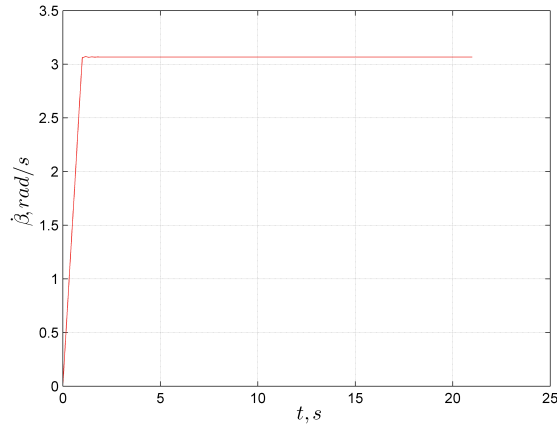
ω_{ref}, $\dot{\omega}_{ref}$ are reference values vectors of general coordinates, I is the vector of currents of DC motors, u_{ref} is the vector of reference voltages of the motor and Θ is the vector of disturbances (vector of varying coefficients of the friction between wheels and ground).

Figures 3 and 4 present the controllers structure for dynamic and kinematic control, respectively. Kinematic controller is assumed to be as in [14].

Fig. 5. Trajectory of angular velocity $\dot{\beta}$ for robot moving around the characteristic point

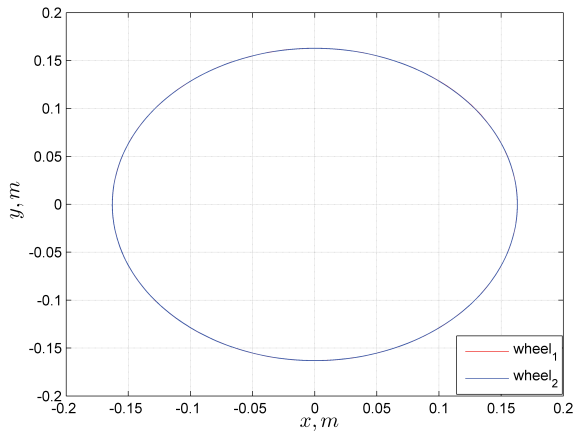Fig. 8. Movement of the characteristic robot point A – dynamic control

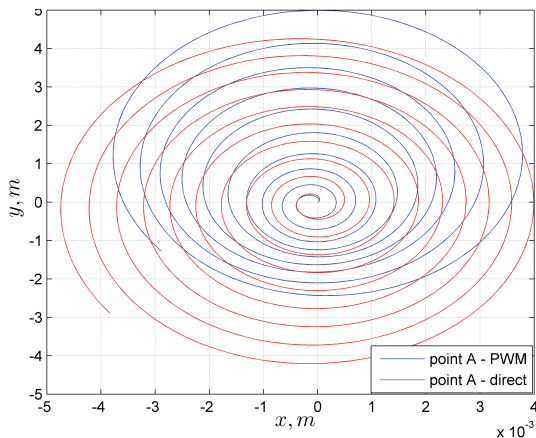Fig. 6. Trajectory of first and second wheel for robot platform moving around the characteristic point A

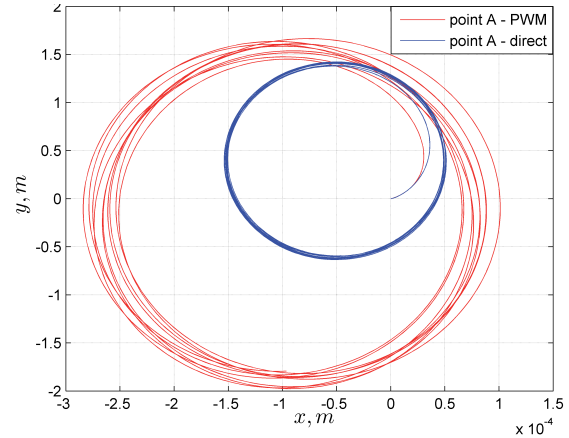Fig. 9. Torque in kinematic trajectory control

Fig. 7. Movement of the characteristic robot point A – kinematic control
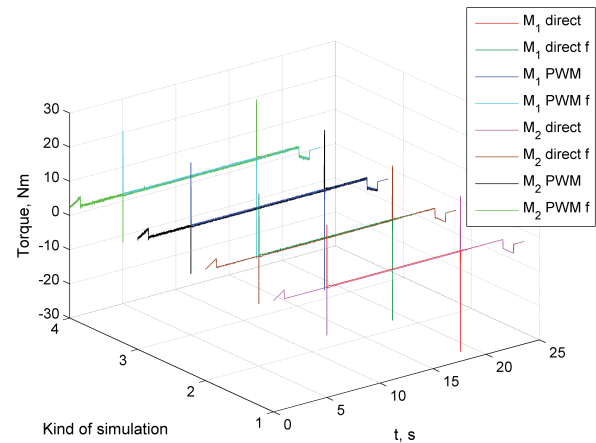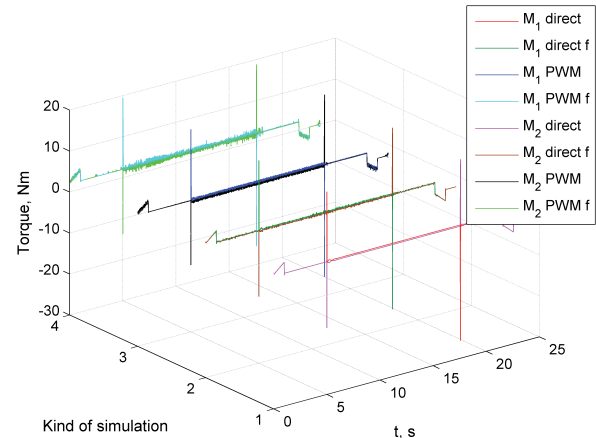

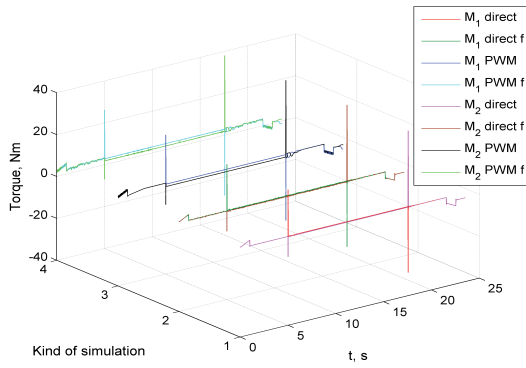Fig. 10. Torque in dynamic trajectory control

Fig. 11. Desired torque in dynamic trajectory control

3. Simulation

The model calibration was inspired with Pioneer 2DX [16] technical parameters:

$$m_5 = 113.4 \, kg, \; m_1 = 1.5 \, kg, \; m_2 = 1.5 \, kg \quad m_3 = 0.5 \, kg,$$

$$I_{z5} = 3.08 \, kg \cdot m^2, \; I_{z1} = 0.052 \, kg \cdot m^2, \; I_{z2} = 0\,052 \, kg \cdot m^2,$$

$$I_{y1} = 0.163 \, kg \cdot m^2, \; I_{y2} = 0.163 \, kg \cdot m^2, \; I_{y3} = 0.07 \, kg \cdot m^2,$$

$$r_1 = 0.0825 \, m, \; r_2 = 0.0825 \, m, \quad r_3 = 0.0211 \, m,$$

$$h_1 = l_1 / r_1, \; l = 0.217 m, \; l_1 = 0.163 m, \; l_2 = 0.07 m,$$

$$l_3 = 0.06 m, \; f_1 = 0.001, \; f_2 = 0.001, \quad f_3 = 1.0.$$

For variable f_1 and f_2, they are assumed to have normal distribution *N(0.001, 0.00058)*. The simulation is carried out for an example trajectory as in [12] and for the robot platform (Fig. 1.) moving around the characteristic point A (Fig. 5).

In the first second, the robot accelerated and then next 20 seconds it was moving with the constant velocities.

We also analyze for both control types in direct torque or voltage control (as exemplary testing base) and the widely known PWM control. This control (with H Transistor Bridge) is the most popular for changing voltages in DC motors.

Figures 6, 7 and 8 show cases when PD controller with gains Kd = 141.0 and Kp = 473.0 is applied. These gains were calculated by means of Hooke-Jevees optimization of the trajectory accuracy [12]. Fig. 7 and Fig. 8 show the movement of the characteristic point A.

4. Simulation results

The errors of the trajectory as in [12] and, for the trajectory with the robot platform moving around the characteristic point A (Fig. 5), were presented in Tables 1 to 4. The errors for the whole trajectory are calculated as follows:

$$\Delta\beta = \sqrt{\frac{1}{n}\sum_{i=1}^{n}(\beta_{di} - \beta_i)^2}, \; \Delta\psi = \sqrt{\frac{1}{n}\sum_{i=1}^{n}(\psi_{di} - \psi_i)^2}, \qquad (13)$$

$$\Delta\dot{\beta} = \sqrt{\frac{1}{n}\sum_{i=1}^{n}(\dot{\beta}_{di} - \dot{\beta}_i)^2}, \; \Delta\dot{\psi} = \sqrt{\frac{1}{n}\sum_{i=1}^{n}(\dot{\psi}_{di} - \dot{\psi}_i)^2}, \qquad (14)$$

where: $\Delta\beta$ – root mean square (RMS) errors of angle β , $\Delta\psi$ – RMS error of angle ψ , $\Delta\dot{\beta}$ – RMS error of velocity $\dot{\beta}$, $\Delta\dot{\psi}$ – RMS error of velocity $\dot{\psi}$, i – an individual
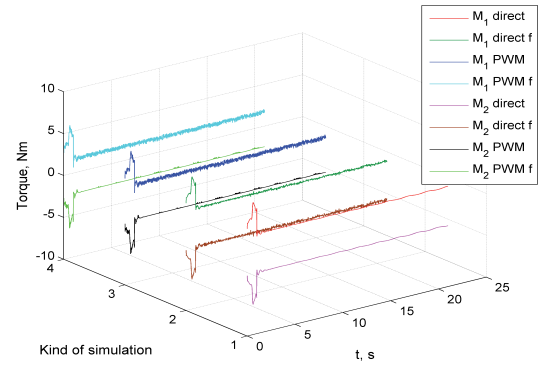

Fig. 12. Torque in kinematic control – moving around
The control types are denoted as follows. 1 stands for direct control, 2 denotes direct control with varying friction coefficients, 3 is PWM control and 4 – PWM control with varying friction coefficients.
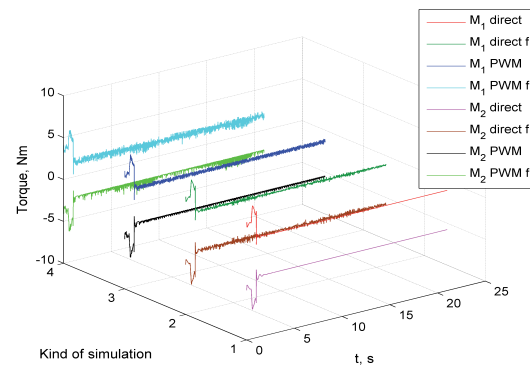

Fig. 13. Torque in dynamic control-moving around

Table 1. Root mean square errors for given in [12] trajectory

Kind of control	Root mean square errors			
	$\Delta\beta$ [rad]	$\Delta\psi$ [rad]	$\Delta\dot{\beta}$ [rad/s]	$\Delta\dot{\psi}$ [rad/s]
Kinematic direct_f	$9.19 \cdot 10^{-2}$	$3.62 \cdot 10^{0}$	$9.58 \cdot 10^{-3}$	$2.61 \cdot 10^{-1}$
Dynamic direct_f	$5.70 \cdot 10^{-4}$	$1.47 \cdot 10^{-4}$	$5.52 \cdot 10^{-3}$	$2.84 \cdot 10^{-3}$
Kinematic direct	$9.19 \cdot 10^{-2}$	$3.62 \cdot 10^{0}$	$5.98 \cdot 10^{-3}$	$2.61 \cdot 10^{-1}$
Dynamic direct	$5.71 \cdot 10^{-4}$	$1.48 \cdot 10^{-4}$	$5.52 \cdot 10^{-3}$	$2.86 \cdot 10^{-3}$
Kinematic PWM	$9.97 \cdot 10^{-2}$	$3.63 \cdot 10^{0}$	$1.02 \cdot 10^{-3}$	$2.62 \cdot 10^{-1}$
Dynamic PWM	$8.08 \cdot 10^{-4}$	$2.49 \cdot 10^{-3}$	$5.70 \cdot 10^{-3}$	$4.13 \cdot 10^{-3}$
Kinematic PWM_f	$9.97 \cdot 10^{-2}$	$3.63 \cdot 10^{0}$	$1.02 \cdot 10^{-2}$	$2.62 \cdot 10^{-1}$
Dynamic PWM_f	$6.55 \cdot 10^{-4}$	$1.76 \cdot 10^{-3}$	$5.70 \cdot 10^{-3}$	$4.27 \cdot 10^{-3}$

step, n – number of steps, index d stands for desired values. The maximum errors were calculated as H – errors, i.e. as a maximum absolute error for the whole trajectory. Angles β and ψ and their angle velocities are equal to:

$$\Delta\beta_{max} = \left|\Delta\beta\right|_\infty, \ \ \Delta\dot\beta_{max} = \left|\Delta\dot\beta\right|_\infty, \quad\quad (15)$$

$$\Delta\psi_{max} = \left|\Delta\psi\right|_\infty, \quad\quad \Delta\dot\psi_{max} = \left|\Delta\dot\psi\right|_\infty, \quad\quad (16)$$

where index *max* denotes the maximum value. Index *f* in tables 1 to 4 means that in this simulation we analyzed the varying wheel friction of the ground.

Table 2. Maximum errors for given in [12] trajectory

Kind of control	Maximum errors			
	$\Delta\beta$ [rad]	$\Delta\psi$ [rad]	$\Delta\dot\beta$ [rad/s]	$\Delta\dot\psi$ [rad/s]
Kinematic direct_f	$1.45\cdot10^{-1}$	$5.94\cdot10^{0}$	$2.50\cdot10^{-1}$	$3.70\cdot10^{-1}$
Dynamic direct_f	$2.16\cdot10^{-3}$	$1.39\cdot10^{-3}$	$2.50\cdot10^{-1}$	$1.08\cdot10^{-1}$
Kinematic direct	$1.45\cdot10^{-2}$	$5.94\cdot10^{0}$	$2.50\cdot10^{-1}$	$3.69\cdot10^{-1}$
Dynamic direct	$2.16\cdot10^{-3}$	$1.39\cdot10^{-3}$	$2.50\cdot10^{-1}$	$1.08\cdot10^{-1}$
Kinematic PWM	$1.57\cdot10^{-3}$	$5.95\cdot10^{0}$	$2.50\cdot10^{-1}$	$3.76\cdot10^{-1}$
Dynamic PWM	$3.06\cdot10^{-3}$	$6.21\cdot10^{-3}$	$2.50\cdot10^{-1}$	$1.08\cdot10^{-1}$
Kinematic PWM_f	$1.57\cdot10^{-1}$	$5.95\cdot10^{0}$	$2.50\cdot10^{-1}$	$3.75\cdot10^{-1}$
Dynamic PWM_f	$2.83\cdot10^{-3}$	$5.19\cdot10^{-3}$	$2.51\cdot10^{-1}$	$1.10\cdot10^{-1}$

Table 3. Root mean square errors for trajectory of robot moving around the characteristic point

Kind of control	Root mean square errors			
	$\Delta\beta$ [rad]	$\Delta\psi$ [rad]	$\Delta\dot\beta$ [rad/s]	$\Delta\dot\psi$ [rad/s]
Kinematic direct_f	$1.64\cdot10^{0}$	$4.57\cdot10^{-2}$	$1.39\cdot10^{-1}$	$3.87\cdot10^{-3}$
Dynamic direct_f	$8.36\cdot10^{-5}$	$3.67\cdot10^{-3}$	$1.91\cdot10^{-3}$	$8.51\cdot10^{-4}$
Kinematic direct	$1.64\cdot10^{0}$	$4.57\cdot10^{-2}$	$1.39\cdot10^{-1}$	$3.87\cdot10^{-3}$
Dynamic direct	$8.36\cdot10^{-5}$	$3.67\cdot10^{-3}$	$1.73\cdot10^{-3}$	$7.67\cdot10^{-4}$
Kinematic PWM	$1.65\cdot10^{0}$	$3.64\cdot10^{-3}$	$1.39\cdot10^{-1}$	$8.26\cdot10^{-4}$
Dynamic PWM	$8.36\cdot10^{-3}$	$6.68\cdot10^{-3}$	$1.81\cdot10^{-3}$	$1.60\cdot10^{-3}$
Kinematic PWM_f	$1.65\cdot10^{0}$	$3.71\cdot10^{-3}$	$1.39\cdot10^{-1}$	$8.26\cdot10^{-4}$
Dynamic PWM_f	$8.34\cdot10^{-3}$	$6.47\cdot10^{-3}$	$1.98\cdot10^{-3}$	$1.84\cdot10^{-3}$

Large errors achieved for simulations with the kinematic control indicate that this control type is insufficient for the mobile robot. As shown in Tables 1 and 3, there is also a significant difference between PWM and a direct voltage control. However, in real models we can use only PWM, as direct control is strictly theoretical. The index
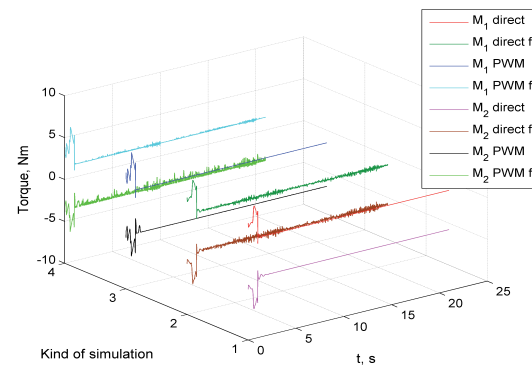

Fig. 14. Desired torque in dynamic control – moving around

f indicates that in the given simulation we analyzed the varying wheel friction of the ground.

Tables 3 and 4 show errors of general coordinates for robot platform moving around the characteristic point A. For this type of motion, the characteristic point A should not move. But with the impact of the sliding castor wheel being considered, the point A moved in the first phase of the motion.

Table 4. Maximum errors for trajectory of robot moving around the characteristic A point

Kind of control	Maximum errors			
	$\Delta\beta$ [rad]	$\Delta\psi$ [rad]	$\Delta\dot\beta$ [rad/s]	$\Delta\dot\psi$ [rad/s]
Kinematic direct_f	$2.88\cdot10^{0}$	$8.03\cdot10^{-2}$	$1.72\cdot10^{-1}$	$4.95\cdot10^{-3}$
Dynamic direct_f	$8.69\cdot10^{-3}$	$3.83\cdot10^{-3}$	$1.46\cdot10^{-2}$	$6.34\cdot10^{-3}$
Kinematic direct	$2.88\cdot10^{0}$	$8.03\cdot10^{-2}$	$1.72\cdot10^{-2}$	$4.22\cdot10^{-3}$
Dynamic direct	$8.57\cdot10^{-3}$	$3.77\cdot10^{-3}$	$1.47\cdot10^{-2}$	$6.01\cdot10^{-3}$
Kinematic PWM	$2.89\cdot10^{0}$	$5.32\cdot10^{-3}$	$1.74\cdot10^{-1}$	$1.17\cdot10^{-2}$
Dynamic PWM	$8.60\cdot10^{-3}$	$6.91\cdot10^{-3}$	$1.70\cdot10^{-2}$	$1.52\cdot10^{-2}$
Kinematic PWM_f	$2.89\cdot10^{0}$	$5.46\cdot10^{-3}$	$1.74\cdot10^{-1}$	$1.18\cdot10^{-2}$
Dynamic PWM_f	$8.66\cdot10^{-3}$	$6.79\cdot10^{-3}$	$1.73\cdot10^{-2}$	$1.51\cdot10^{-2}$

Results shown in Table 3 and 4 are encouraging, because, for the robot moving around the characteristic point A, the varying friction does not influence the trajectory. In figures below, M_1 *direct*, M_2 *direct* stand for torques for theoretical direct voltage control. M_1 *PWM* and M_2 *PWM* denote torques for PWM voltage control.

Even though the simulation results for mobile robot moving along the trajectory as in [12] seem to be almost identical as presented Fig. 9-11, results presented in tables 1 and 2 leave no doubt that the kinematic control causes greater deviations compared to dynamic control. For comparison, we present the set torques (Fig. 10). Fig. 12, 13 and 14 show the torque of mobile robot when rotating around its a fixed axis (characteristic point A).

Fig. 12 and 13 depict theoretical torques for kinematic and dynamic control, from which, when compared to Fig. 14 showing the set torques, we can conclude that for kinematic control the torques are less oscillatory as compared to dynamic control. The reason for this is the impact of angle velocity regulation in dynamic control, which causes a greater sensitivity of the automatic regulation system.

5. Conclusion

In Fig. 9 to 14, we show torques for kinematic and dynamic control types, with and without PWM. We also show the impact of the varying friction coefficient on the trajectory accuracy.

The kinematic controller is not suitable for high accuracy control of the mobile robot, because in our model with a castor sliding wheel the kinematic controller cannot stabilize the motion, as the errors in kinematic control are too large. Such magnitude of errors might have been triggered with too large time constant of the regulator. Given this, the kinematic control should not be applied for mobile robots, as it brings about significant trajectory errors. Our results are conductive for improving the robot simulation procedure so as to achieve results closer to robot behavior in reality.

Acknowledgements

AUTHORS

Ryszard Beniak* – Opole University of Technology, Faculty of Electrical Engineering, Automatic Control and Computer Science, Prószkowska Street No. 76, 45-758 Opole, Poland,
e-mail: r.beniak@po.opole.pl

Tomasz Pyka – Opole University of Technology, Faculty of Electrical Engineering, Automatic Control and Computer Science, Prószkowska Street No. 76, 45-758 Opole, Poland,
e-mail: t.pyka@doktorant.po.edu.pl

*Corresponding author

References

[1] R. Balakrishna and A. Ghosal, "Modelling of Slip for Wheeled Mobile Robots", *IEEE Transactions on Robotics and Automation*, vol. 11, no. 1, February 1995.

[2] Xiaocai Zhu *et al.*, "Robust Tracking Control of Wheeled Mobile Robots Not Satisfying Nonholonomic Contraints". In: *Proceedings of the 6th International Conference on Intelligent Systems Design and Applications (ISDA'06),* 2006.

[3] Y. P. Li, T. Zielinska, M. H. Jr Ang and W. Lin, "Vehicle dynamics of redundant mobile robots with powered caster wheels", *Proceedings of the Sixteenth CISM-IFToMM Symposium, Romansy 16, Robot Design, Dynamics and Control,* Warsaw: Springer, 2006, pp. 221–228.

[4] K. Zdanowska, A. Oleksy, "Motion planning of Wheeler mobile robots subject to slipping", *Journal of Automation, Mobile Robotics & Intelligent Systems*, vol. 5, no. 3, 2011.

[5] Ch. C. Ward and K. Iagnemma, "Model-Based Wheel Slip Detection for Outdoor Mobile Robots", *IEEE International Conference on Robotics and Automation* Roma, Italy, April 2007.

[6] D. DeVon and T. Bretl, "Kinematic and Dynamic Control of a Wheel Mobile Robot", *Proceedings of the 2007 IEEE/RSJ International Conference on Intelligent Robots and Systems San Diego, CA, USA*, 29th Oct. – 2nd Nov. 2007.

[7] N. Sidek and N. Sarkar, "Dynamic Modeling and Control of Nonholonomic Mobile Robot with Lateral Slip", *Proceedings of the 7th WSEAS International Conference on Signal Processing, Robotics and Automation (ISPRA'08)*, 2008.

[8] Yin-Tien Wang,Yu-Cheng Chen and Ming-Chun Lin, "Dynamic Object Tracking Control for a Non-Holonomic Wheeled Autonomous Robot", *Tamkang Journal of Science and Egineering*, vol. 12, no. 3, 2009, pp. 339–350.

[9] N. Sidek, N. Sarkar, "Inclusion of Wheel Slips in Mobile Robot Modeling to Enhance Robot Simulator Performance", *The 3rd Int. Conf. on Mechatronics (ICOM 08)*, 18th–20th Dec. 2008.

[10] R. Dayal Parhi and B. B. V. L. Deepak: "Kinematic model of three wheeled mobile robot", *Journal of Mechanical Engineering Research,* vol. 3(9), 2011, pp. 307–318.

[11] F.N. Martins, W.C. Celeste, R. Carelli, M. Sarcinelli-Filho, T.F. Bastos-Filho, "An adaptive dynamic controller for autonomous mobile robot trajectory tracking", *Control Engineering Practice*, vol. 16, 2008, pp. 1354–1363.

[12] R. Beniak, T. Pyka, "Selection of controller setpoints for a tri-wheel robot taking into account the impact of the dragged wheel and varying coefficients of wheel friction", *The Measurements, Automation and Monitoring,* no. 11, 2010. pp. 1390–1395. (in Polish)

[13] M. Kaźmierkowski, R. Krishnan, F. Blaabjerg, "Control in Power Electronics", *Academic Press an impring of Elsevier Science*, 2002.

[14] L. Gracia, J. Tornero, "Kinematic control of wheeled mobile robots", *Latin American Applied Research,* vol. 38, no. 1, pp. 7–16.

[15] R. Beniak, T. Pyka, "Control stepsize optimization for tri-wheel mobile robot", *3rd International Students Conference Electrodynamics and Mechatronics,* Opole, 2011.

[16] M. J. Giergiel, Z. Hendzel, W. Żylski, "Modeling and control of wheeled mobile robots", Warsaw: Polish Scientific Publishers PWN, 2002. (in Polish).